

Photon collection from a trapped ion–cavity system

J. D. Sterk,^{1,*} L. Luo,^{1,†} T. A. Manning,¹ P. Maunz,² and C. Monroe¹

¹*Joint Quantum Institute, University of Maryland Department of Physics and
National Institute of Standards and Technology, College Park, MD 20742*

²*Fitzpatrick Institute for Photonics, Department of Electrical and Computer Engineering, Duke University, Durham, NC 27708*
(Dated: October 29, 2018)

We present the design and implementation of a trapped ion cavity QED system. A single ytterbium ion is confined by a micron-scale ion trap inside a 2 mm optical cavity. The ion is coherently pumped by near resonant laser light while the cavity output is monitored as a function of pump intensity and cavity detuning. We observe a Purcell enhancement of scattered light into the solid angle subtended by the optical cavity, as well as a three-peak structure arising from strongly driving the atom. This system can be integrated into existing atom–photon quantum network protocols and is a pathway towards an efficient atom–photon quantum interface.

I. INTRODUCTION

Quantum networks rely upon an efficient interface between the quantum memories and the photonic channels used for remote entanglement. Trapped ions are a standard platform to realize a quantum network due to their long coherence times and the availability of high fidelity quantum gate operations [1, 2]. Current implementations of trapped ion based quantum networks have demonstrated the ability to entangle remote nodes, violate Bell’s inequality, perform teleportation, realize remote quantum gates, and generate private random numbers [3–7]. In these experiments, the interface between the ion and the photonic channel depends upon a probabilistic process wherein the scattered photon is collected by a microscope objective subtending only a small fraction of the emission solid angle.

There has been recent interest in integrating optical elements with an ion trap system to improve the photon collection efficiency. Nearby optics such as a fiber tip [8], reflective mirror [9, 10], or Fresnel lens [11, 12] can have larger numerical apertures than common microscope objectives. Additionally, integrating multi-scale optics—such as microfabricated mirrors—with ion traps may provide a path towards scaling up a trapped ion network [13, 14]. Although these methods increase the collection efficiency, they are still inherently probabilistic in nature.

Coupling a trapped ion to an optical cavity can lead to a very high photon collection efficiency. In principle, with a large coupling strength between an ion and a cavity, the photon collection efficiency can approach unity [15, 16]. Since the cavity mode interacts coherently with the atomic state, this process is reversible and can be used for generating quantum networks [17]. Experiments with neutral atoms—where transition frequen-

cies are typically in the infrared—have demonstrated efficient atom–photon interfaces as well as atom–photon and photon–photon entanglement [16, 18, 19].

Efforts toward coupling trapped ions to optical cavities have used infrared frequency transitions to a metastable D state for the optical cavity [20–23]. At these wavelengths, high finesse mirrors are available and strong coupling can be achieved. Single photons can be efficiently generated in this system using techniques similar to neutral atom cavity QED experiments [22, 23]. However, these methods do not integrate directly with currently demonstrated trapped ion quantum network protocols.

In this paper, we detail the design and fabrication of a trapped ion system where a single ytterbium ion is coupled to a moderate-finesse optical cavity resonant with the ultraviolet $S_{1/2} \leftrightarrow P_{1/2}$ transition at 369.5 nm. Such a system could couple to individual hyperfine levels of the ytterbium qubit and be integrated into existing atom–photon quantum network protocols [24]. We trap a single $^{174}\text{Yb}^+$ ion inside the cavity and coherently pump it with a laser from the side of the cavity while monitoring the cavity output. The photon scatter rate into the solid angle subtended by the cavity mode in the outcoupling direction is enhanced by a factor of 600. Additionally, the spectral properties of the atomic emission are observed as we detune the cavity from the atomic resonance. At large pump strengths, an emergence of a three-peak structure from the spectrum of emitted light indicates a Mollow triplet on a single atom level.

II. EXPERIMENTAL SYSTEM

A single ytterbium ion is confined by a radiofrequency (RF) ion trap inside the mode of an optical cavity resonant to the $S_{1/2} \leftrightarrow P_{1/2}$ transition at 369.5 nm. To couple the ion to the optical cavity, we developed a novel micron-scale ion trap that can be inserted into the cavity mode *in situ*. A nearby RF ground is an order of magnitude closer to the ion than the dielectric mirrors to mitigate effects of dielectric charging [25].

* Present Address: Sandia National Laboratories, Albuquerque NM 87185; jdsterk@sandia.gov

† Present Address: Department of Physics, Indiana University–Purdue University Indianapolis, Indianapolis IN 46202

A. Optical cavity design, fabrication, and test

The optical cavity consists of a pair of highly reflective concave mirrors from Advanced Thin Films set up in a near-planar Fabry-Pérot configuration. The mirrors were initially 7.75 mm in diameter and 4 mm thick when coated. After coating, the mirrors were coned to a 2 mm diameter reflective surface and 4 mm outer diameter. The radius of curvature of the mirrors is 25 mm.

At ultraviolet frequencies, optical coating losses are two orders of magnitude larger than infrared frequencies. The absorption and scattering losses for our cavity initially was ≈ 400 ppm. The mirrors form an asymmetric cavity with an outcoupling mirror transmission of $T_{\text{out}} \approx 1000$ ppm, which is larger than the incoupling mirror (set to $T_{\text{in}} \approx 200$ ppm). Because the ultraviolet light for Doppler cooling and coherently pumping the ion is derived from a frequency doubled diode laser, the mirrors were additionally coated for 739 nm for cavity length stabilization (cf. Sec. II C).

The free spectral range of the optical cavity was measured to be 70.5 GHz by scanning the 739 nm laser across consecutive transmission peaks. This corresponds to a cavity length of 2.126 mm. The full-width at half-maximum was measured by scanning the cavity length across resonance and using the frequency difference between acousto-optic modulator (AOM) orders as a frequency marker [26]. The measured full-width at half-maximum was $\kappa/\pi = 18.6$ MHz, corresponding to a finesse of $\mathfrak{F} = 3790$, and an outcoupling efficiency of 0.6.

However, we noticed that the finesse of our cavity degraded after running the experiment for several weeks. To our knowledge, several other groups have noticed a similar effect in their ultraviolet cavities [27, 28]. A direct measurement of the cavity linewidth was made by driving the cavity mode at a fixed laser frequency and scanning the cavity length across resonance. After attenuation of the output, photon counts are measured on a photomultiplier tube (PMT). The increased linewidth is $\kappa/\pi = 47.4$ MHz, corresponding to a finesse of $\mathfrak{F} = 1490$ and outcoupling efficiency of 0.24. The relevant cavity QED parameters for our system are thus $(g, \kappa, \gamma)/2\pi = (3.92, 23.7, 19.6)$ MHz, which gives a single-atom cooperativity of $C = g^2/\kappa\gamma = 0.033$. Due to the comparable strengths of the parameters, our system lies in the intermediate regime of cavity QED [29, 30].

B. Ion trap for enhanced light collection

Our cavity QED system requires an optically open ion trap where the ion can be precisely placed inside the optical mode. The RF quadrupole trap is a modified version of an earlier design, where the ion trap electrodes can be adjusted independently [31]. The designed trap consists of two identical laser machined alumina substrates with lithographically patterned electrodes (Figure 1). Each substrate is mounted on a linear positioner inside the

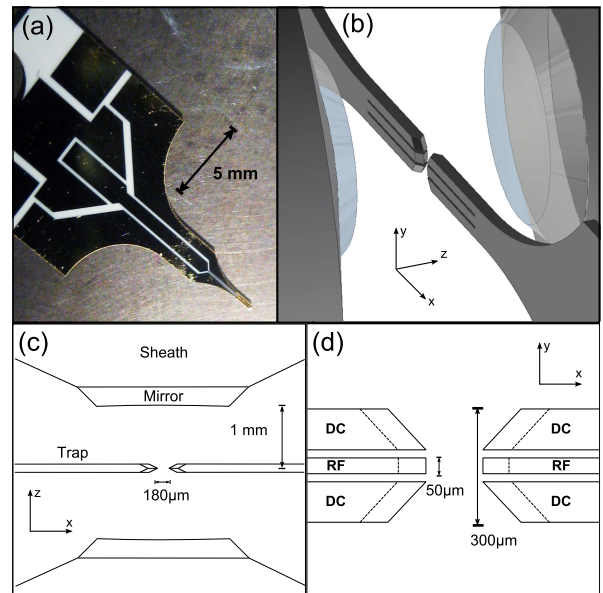


FIG. 1. Trap electrode and cavity geometry. (a) Photograph of a substrate ready for wiring. (b) Two identical substrates are inserted between the cavity mirrors such that the ion resides in the cavity mode. (c) A top view of the ion trap inside the cavity. The substrates are separated by $180\ \mu\text{m}$ and are 1 mm from the mirror. The mirrors are mounted in metal sheaths to provide compensation along the cavity direction. (d) The tapered tip is machined to three individual tines. The outer tines are RF ground and provide compensation fields, while the center tine is RF high.

vacuum chamber such that the position of the ion trap can be placed inside the cavity mode *in situ*.

Figure 1a is a photograph of a finished substrate. Each substrate is laser machined to a narrow finger approximately $300\ \mu\text{m}$ wide. This finger is further machined into three individual tines, as illustrated in Fig. 1d. The outer tines are approximately $100\ \mu\text{m}$ wide and provide a nearby RF ground. The center tine is approximately $50\ \mu\text{m}$ wide and is at RF high. The gaps between the tines are about $25\ \mu\text{m}$, and the tips are beveled on both sides to minimize surface area visible to the ion. The back portion of the electrodes provides enough space for on-board RF filters that are wire bonded onto the substrate. Gold is evaporated onto the surface of the substrate up to a thickness of $1\ \mu\text{m}$. A particular lithographic process was developed to ensure gold was coated around the entire substrate tip.

Stray electric fields can be compensated by applying static DC offset voltages to the outer tines. To compensate for stray fields along the cavity axis, we apply a DC voltage on metal sheaths placed around the cavity mirrors as shown in Figure 1c.

To avoid diffractive losses in the cavity mode due to the presence of the ion trap, the trap separation was chosen to be $180\ \mu\text{m}$, which is greater than three times the mode diameter $2w_0 = 50\ \mu\text{m}$. At this separation, the reduc-

tion in trap confinement compared to an ideal hyperbolic electrode trap of the same characteristic size—known as the voltage efficiency factor η —is 0.45. We apply 300 V of RF at 21.6 MHz, and observe secular frequencies of 4 MHz.

The secular frequencies are measured by resonantly driving the secular motion of the ion with a sinusoidal voltage on one of the outer tines. While monitoring the ion motion on a CCD camera, the frequency of the voltage is swept across the motional resonances. From the orientation of the motion on the camera, we are able to discriminate between motion along the cavity axis and along the trap axis.

We perform this measurement as a function of ion trap separation as well as a DC bias voltage on the RF electrodes. To lowest order, the secular frequencies of the trap are given by

$$\omega_i = \sqrt{\frac{eU_0Q_i}{m} + \frac{1}{2} \left(\frac{eV_0Q_i}{m\Omega} \right)^2}, \quad (1)$$

where Q_i is the quadrupole moment of the trap potential in the i -th direction. Since the quadrupole moment is traceless, we note that $Q_x + Q_y + Q_z = 0$. Along the electrode axis, the quadrupole moment is $Q_x = \eta/x_0^2$, where $2x_0$ is the separation of the trap electrodes. The voltage on the RF electrode consists of a DC bias U_0 and RF voltage V_0 at frequency Ω . Figures 2a–d illustrates the measured secular frequencies for various separations and bias voltages. The solid lines are fits to the data, providing good agreement with equation 1. From the data, we are able to extract the voltage efficiency factor for various separations and compare it to a numerical simulation of the trap (Figure 2e).

C. Experimental Setup

A diagram of the experimental apparatus is shown in Fig. 3. The ion trap substrates are attached to individual linear positioners, allowing them to be placed inside the cavity mode with micron-level precision. To coarsely align the ion to the cavity mode, the cavity is repeatedly scanned over resonance with 739 nm light pumping the cavity. The transmission peaks are monitored as the electrodes are inserted into the cavity mode. Loss of transmission indicates a rough estimate of the position of the mode. Finer adjustment of the ion position is made by pumping the cavity with ultraviolet light and increasing the photon scatter from the ion out the side of the cavity. The final method of improvement of ion–cavity coupling is an iterative process where the fluorescence out the cavity is monitored and maximized.

A thermal beam of ytterbium is produced by resistive heating of a stainless steel tube in which Yb metal is packed. To minimize the probability of coating the cavity mirrors with ytterbium, current is run through the ovens slightly above the threshold to produce ytterbium atoms.

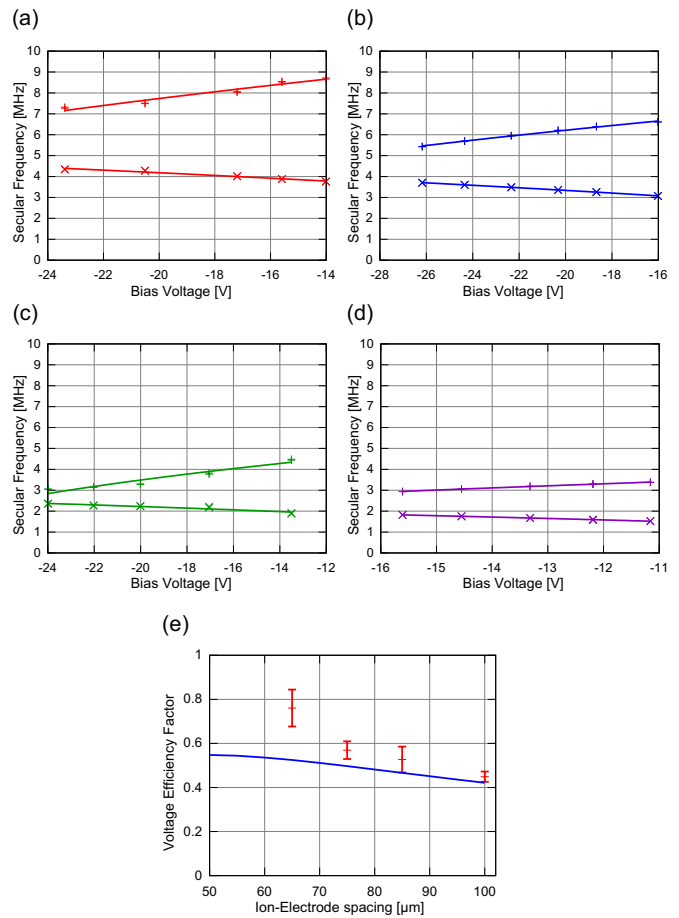


FIG. 2. Electrical characterization of our trap. The secular frequency of the trap is measured for various bias voltages U_0 and trap separations. Crosses (×) indicate frequencies along the trap axis, while (+) indicate frequencies along the cavity axis. Solid lines indicate fits to equation 1. Electrode separations are: (a) $2x_0 = 130$ μm, (b) 150 μm. (c) 170 μm. (d) 200 μm. (e) The voltage efficiency factor from our measurements is compared to numerical simulations.

Additionally, the thermal beam of atoms is perpendicular to the cavity axis. Ions are produced by a resonantly enhanced two-photon transition to the continuum with a 398.9 nm and 369.5 nm beam [32].

The ions are cooled on the $S_{1/2} \leftrightarrow P_{1/2}$ transition of $^{174}\text{Yb}^+$ at 369.5 nm by a frequency doubled diode laser at 739 nm. A 935.2 nm beam is used to repump the ion out of a low-lying $D_{3/2}$ level, which has a lifetime (52.7 ms) longer than the measurement time. To measure the background light, the repump light is turned off with an AOM.

The optical cavity is stabilized through a Pound–Drever–Hall locking technique with 200 μW of 739 nm light at a frequency ν_{ir} . Due to the Gouy phase shift and differences in the indices of refraction of the optical coating at 739 nm and at 369.5 nm, the second harmonic $2\nu_{\text{ir}}$ is not resonant with the cavity. From the resonance

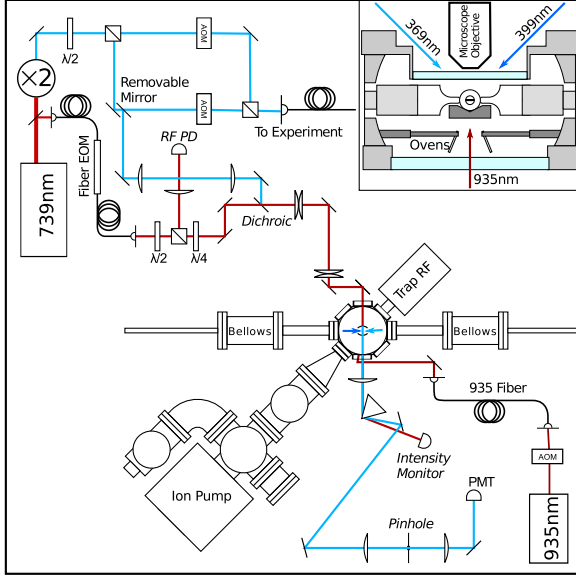


FIG. 3. The experimental system consists of a diode laser at 739 nm that is frequency doubled to drive the atom. The two arms of the 369.5 nm light are combined into a fiber that delivers the cooling and pump light to the ion. The cooling and pump are toggled during the experiment, allowing the pump to vary in intensity while keeping the cooling constant. The cavity is stabilized to the fundamental at 739 nm. A fiber electro-optic phase modulator (EOM) provides tunability of the cavity resonance as well as the necessary frequency offset to ensure co-resonance of the beams. (*Top Right*) A side view schematic along the cavity axis indicating the locations of the cooling/pump beam, the ionization beam, and the repump beam. The ion is imaged from above.

condition of the q -th longitudinal mode of a symmetric optical cavity of length L and mirror radii of curvature \mathcal{R} [33],

$$\pi q = \frac{2\pi\nu_q L}{c} - \arccos\left(1 - \frac{L}{\mathcal{R}}\right), \quad (2)$$

we find the ultraviolet resonance ν_{uv} to be shifted from the harmonic of the infrared resonance by an amount $\Delta f = \nu_{ir} - \frac{1}{2}\nu_{uv}$ to be

$$\Delta f = \nu_{ir} \frac{L_{uv} - L_{ir}}{L_{uv}} + \frac{c}{2\pi L_{uv}} \left[\phi_{ir} - \frac{1}{2}\phi_{uv} \right]. \quad (3)$$

In equation 3, we take the cavity lengths in the ultraviolet and infrared to be L_{uv} and L_{ir} , and the Gouy phase $\phi_{ir(uv)} = \arccos\left(1 - \frac{L_{ir(uv)}}{\mathcal{R}_{ir(uv)}}\right)$. For our cavity, we find there to be a 2.3 GHz frequency offset of the infrared light to reach the resonance of the ytterbium ion, corresponding to a length difference of approximately 12 nm. The offset is provided by a wide-bandwidth fiber EOM. This modulator additionally gives us independent control of the cavity resonance with respect to the laser frequency.

With the cavity locked, both ultraviolet light from the ion and infrared light exit the cavity. After an initial col-

imating lens, the output of the cavity is sent through a prism to separate the colors (Figure 3). The infrared light is sent onto a photodiode to monitor the cavity transmission, while the ultraviolet beam is spatially filtered and directed onto a PMT. The overall efficiency of our detection system (including detector quantum efficiency) is 4%.

III. EXPERIMENTAL RESULTS

The experimental procedure is as follows. The ion is Doppler cooled for 20 ms with a weak cooling beam. Next, a strong pump beam is turned on for 2 ms and photon counts out of the cavity are recorded. For half the detection time, the 935 nm repump light is off, providing a measurement of the background light for subtraction. We average over 40 measurement cycles before changing the cavity frequency. In this manner, a lineshape is built up for a set pump intensity. The strong pump is detuned from atomic resonance by 10 MHz to avoid heating of the ion during the measurement.

The power of the coherent pump is calibrated by ion fluorescence from the side of the cavity. The ion fluorescence is collected by a microscope objective and imaged onto a PMT. By measuring the scatter rate out the side of the cavity for various input powers, the intensity at the ion versus the input power can be determined in terms of the saturation intensity.

When the cavity is resonant, we observe up to 8000 photon counts per second on the PMT. Our PMT has a quantum efficiency of 19% and the prism has a transmission of 23.5%. Given these efficiencies in the detection path, our measured value corresponds to 200,000 photons emerging from the cavity per second. From our estimated outcoupling efficiency of 0.24, we estimate the cavity collects 800,000 photons per second. Table I summarizes the efficiencies and backs out the photon scatter rate into the cavity. The photon emission rate agrees with the estimate that the emission rate is given by $p_{coll}\Gamma_{sc}$, where p_{coll} is the collection probability given by [24]

$$p_{coll} = \frac{T_{out}}{\mathcal{L}} \left(\frac{2\kappa}{2\kappa + \gamma} \right) \left(\frac{2C_{eff}}{1 + 2C_{eff}} \right) \quad (4)$$

and Γ_{sc} is the photon scatter rate. Here, T_{out}/\mathcal{L} is the outcoupling efficiency while $2\kappa/(2\kappa + \gamma)$ is the ratio of the rate at which the photon leaves the cavity to the total rate at which the ion-cavity system loses photons. The third factor, $2C_{eff}/(1 + 2C_{eff})$, is the Purcell enhancement with an effective cooperativity C_{eff} for a reduced coherent coupling rate due to averaging of the atomic motion across the cavity standing wave.

To compute the enhancement in photon collection efficiency, we compare our result to isotropic scattering of photons from a single ytterbium ion. We define the enhancement to be the ratio of photons emerging from the cavity to the isotropic scatter rate into the solid angle

| | Efficiency | Count rate |
|------------------------|------------|----------------------------------|
| Detected | | 8000 s^{-1} |
| Before PMT | 0.19 | $42,000 \text{ s}^{-1}$ |
| Before Prism | 0.235 | $180,000 \text{ s}^{-1}$ |
| Before vacuum window | 0.9 | $200,000 \text{ s}^{-1}$ |
| Outcoupling efficiency | 0.24 | $\approx 800,000 \text{ s}^{-1}$ |

TABLE I. List of efficiencies and the effective photon scatter rates before elements. There are approximately 800,000 photons scattered into the cavity per second, where only 200,000 photons/sec emerge from the cavity.

of the cavity mode in outcoupling direction. The solid angle subtended by the cavity mode is given by

$$\Delta\Omega_{\text{cav}} = \frac{2\lambda^2}{\pi w_0^2} = 1.465 \times 10^{-4} \text{ sr} \quad (5)$$

which is twice the solid angle subtended by the mode in the outcoupling direction. We calculate the photon scatter rate for isotropic scattering into this solid angle for the parameters where we observe maximal counts on our PMT. We estimate that without enhancement we would observe 300 photons per second scattered into the outcoupling direction of the cavity mode.

This yields a spontaneous emission enhancement factor of 600 compared to the free-space value into the same solid angle of the cavity mode in the outcoupling direction. Other cavity QED experiments in the intermediate regime of cavity QED have reported an enhancement of 18.5 of spontaneous emission into an undriven cavity mode. This was achieved by delivering cold atoms from a magneto-optical trap into the cavity [34]. Due to the strong confinement of our atom, our system achieves a much higher enhancement of spontaneous emission than any other experiment in the intermediate regime.

In our experiment, we measure the photon counts from the cavity as a function of the cavity detuning $\delta_c = \omega_c - \omega_L$. The fiber EOM offset allows us to set the cavity resonance independently of the pump frequency. We set the atom-laser detuning $\delta_0 = \omega_0 - \omega_L$ to be 10 MHz below resonance, and measure the count rate versus the cavity detuning. Figure 4 illustrates the lineshapes observed for the coherently driven atom for various pumping strengths ($I/I_{\text{sat}} = 2, 50, 150, 600$). At low intensities, we observe a Lorentzian lineshape consistent with a cavity broadened emission line. For strong pump intensities we observe the emergence of a three-peak structure characteristic of the Mollow triplet [35].

We attribute this three-peak structure to a cavity-broadened fluorescence spectrum of the ion. However, the fluorescence spectrum of a two level atom cannot fully describe our data. Instead, the Zeeman levels with various driving strengths must be taken into account. The 174 isotope of ytterbium has zero nuclear spin, and therefore has no hyperfine structure. The $S_{1/2}$ and $P_{1/2}$ manifolds each consist of two nearly degenerate Zeeman states, split by a weak magnetic field perpendicular to the cavity

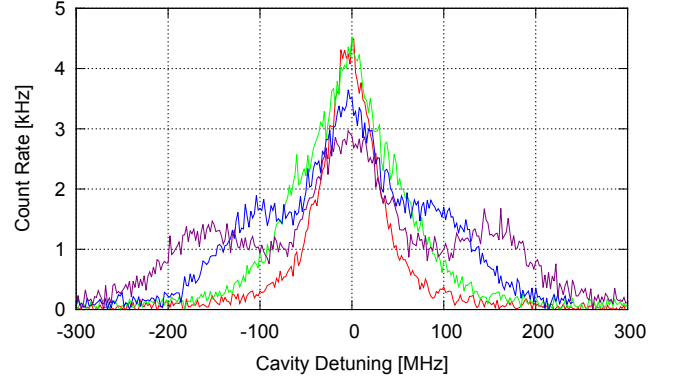


FIG. 4. Steady-state photon count rate from the cavity versus cavity detuning for several drive intensities. At intensities large compared to the saturation intensity, we observe the onset of a triplet structure. Red: $I/I_{\text{sat}} = 2$, Green: $I/I_{\text{sat}} = 50$, Blue: $I/I_{\text{sat}} = 150$, Purple: $I/I_{\text{sat}} = 600$.

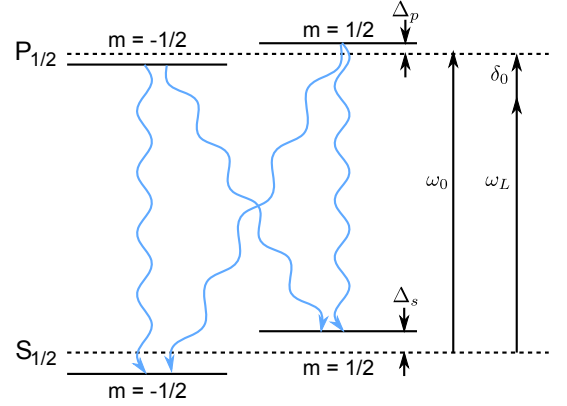


FIG. 5. Relevant atomic energy levels for the $^{174}\text{Yb}^+$ ion. The Zeeman levels are shifted by $\pm\hbar\Delta_{s,p}$. The pump light is detuned from the bare resonance by δ_0 , and the cavity detuning is $\delta_c = \omega_c - \omega_L$.

axis (Figure 5).

We label the four levels of interest as $\{|S_{1/2}, \pm\rangle, |P_{1/2}, \pm\rangle\}$, where $S_{1/2}(P_{1/2})$ corresponds to the ground (excited) state manifold. In a frame rotating at the classical drive frequency ω_L , the atomic Hamiltonian is

$$H_a = \hbar \sum_{\ell, m} \Delta_{\ell} |\ell, m\rangle \langle \ell, m| + \hbar \delta_0 \sum_m |e, m\rangle \langle e, m| \quad (6)$$

where $\pm\Delta_{s(p)}$ is the Zeeman level shift of $|S_{1/2}(P_{1/2}), \pm\rangle$. The second term is the energy of the excited state manifold in the rotated frame, where $\delta_0 = \omega_0 - \omega_L$. The classical driving field, $\mathbf{E} = \frac{1}{2} E_0 \epsilon e^{-i\omega_L t} + c.c.$, can drive all three types of transitions in the ion ($\Delta m = \pm 1, 0$), depending on the orientation of the polarization vector ϵ with respect to the magnetic field. The interaction

Hamiltonian with the classical field can be written as

$$H_d = -\frac{\hbar\Omega}{2} \left[\hat{\mathbf{A}} \cdot \boldsymbol{\epsilon} + \hat{\mathbf{A}}^\dagger \cdot \boldsymbol{\epsilon} \right] \quad (7)$$

where $\Omega = \mu E_0 / \hbar = \gamma \sqrt{I/2I_{\text{sat}}}$ is the Rabi frequency for the $S_{1/2} \leftrightarrow P_{1/2}$ transition, and the lowering operator is

$$\hat{\mathbf{A}} = \sum_{q,m,m'} \langle S_{1/2}, m; 1, q | P_{1/2}, m' \rangle | S_{1/2}, m \rangle \langle P_{1/2}, m' | \mathbf{e}_q \quad (8)$$

with \mathbf{e}_q being the spherical basis vector. The saturation intensity for the $S_{1/2} \leftrightarrow P_{1/2}$ transition is $I_{\text{sat}} = \hbar\omega_0^3\gamma/12\pi c^2 = 50.7 \text{ mW/cm}^2$. The vector component \hat{A}_q describes the transition between the magnetic sublevels m and $m-q$ and is proportional to the Clebsch-Gordan coefficient of that transition [36].

Additionally, we consider the two degenerate polarization modes of the cavity at a frequency ω_c detuned from the drive frequency by $\delta_c = \omega_c - \omega_L$. The Hamiltonian for the two cavity modes in the rotating frame is

$$H_c = \hbar\delta_c \sum_{p=H,V} \hat{a}_p^\dagger \hat{a}_p. \quad (9)$$

The Jaynes-Cummings cavity interaction consists of the coupling of the three atomic transitions to the two cavity modes, and is given by

$$H_{jc} = i\hbar g \sum_{p=H,V} \left[\hat{a}_p^\dagger (\hat{\mathbf{A}} \cdot \mathbf{e}_p^*) - (\hat{\mathbf{A}}^\dagger \cdot \mathbf{e}_p) \hat{a}_p \right] \quad (10)$$

The steady-state photon count rate is given by the steady-state intracavity photon number for both polarizations and the cavity decay rate: $2\kappa [\langle n_H \rangle_{ss} + \langle n_V \rangle_{ss}]$. To compute the intracavity photon number, we numerically solve the master equation

$$\begin{aligned} \dot{\rho} = & -i[\rho, H_a + H_d + H_c + H_{jc}] \\ & + \gamma \sum_q \left[\hat{A}_q \rho \hat{A}_q^\dagger - \frac{1}{2} (\hat{A}_q^\dagger \hat{A}_q \rho + \rho \hat{A}_q^\dagger \hat{A}_q) \right] \\ & + 2\kappa \sum_p \left[\hat{a}_p \rho \hat{a}_p^\dagger - \frac{1}{2} (\hat{a}_p^\dagger \hat{a}_p \rho + \rho \hat{a}_p^\dagger \hat{a}_p) \right] \end{aligned} \quad (11)$$

in steady state using the Quantum Optics Toolbox for MATLAB [37] with our experimental values. The numerical calculation is performed for various detunings of the cavity, and parameters of the classical beam (intensity, orientation relative the magnetic field, and polarization). We fit the data to these simulations and achieve qualitative agreement. A typical fit curve is illustrated in Figure 6, where the parameters for the classical beam are $I = 600I_{\text{sat}}$, oriented 45° from the magnetic field with linear polarization tilted 35° from the cavity axis.

Previously, strongly-driven atoms in a cavity QED system have been studied by passing an atomic beam into an optical cavity, where the Mollow triplet has been observed through the cavity output [38]. Extending such

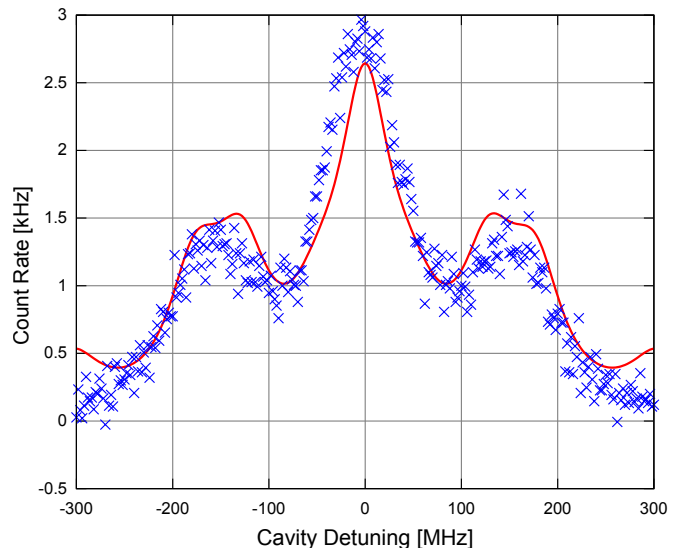


FIG. 6. Typical fit to our data. The solid curve is a numerical calculation of the steady-state intracavity photon number of our cavity versus cavity detuning $\delta_c/2\pi$. Taking into account the Zeeman levels in $^{174}\text{Yb}^+$, we reach qualitative agreement with the observed data.

experiments to a single trapped atom can achieve significant vacuum field dressed-state pumping and steady-state inversion [39–41]. However, such experiments have never been done in trapped neutral atom cavity QED experiments due to the relatively weak confinement compared to the atomic recoil. The strong confinement of our trapped ion allows us to observe the Mollow triplet transition coupled to a cavity at the single atom level for the first time. These results open the way towards studying cavity QED physics with trapped atoms in a strongly-driven regime. Superconducting qubits in a circuit QED system have recently been used to study similar physics [42].

IV. CONCLUSION

We have designed and fabricated a trapped ion cavity QED system where we observe a Purcell enhancement of scattered light into the cavity mode. The scatter rate is two orders of magnitude larger than the scatter rate into the solid angle subtended by the optical cavity. Additionally, we have investigated the photon count rate from the cavity as a function of the cavity detuning and the pump strength. We have found at high intensities, the steady-state count rate exhibits a three-peak structure characteristic of a Mollow triplet. Numerical models of a $^{174}\text{Yb}^+$ ion coupled to an optical cavity yield qualitative agreement with our data.

Additionally, we observe a degradation of the cavity finesse at ultraviolet frequencies. This unexpected effect is possibly a materials related issue and requires more

study. Even at a distance of one millimeter from the ion, the presence of the mirror had a noticeable influence on the ion position, as evidenced by a dynamic and variable stray electric field. This necessitates better shielding and possibly a cavity in a near-concentric configuration which would allow a larger mirror spacing while maintaining the small mode volume required for adequate atom-cavity coupling.

Nevertheless, the enhancement of scattered light into the cavity mode demonstrates the feasibility of increasing the photon collection efficiency for quantum networks. Such an ion-cavity system can be readily integrated into current protocols for trapped-ion quantum networks, providing a pathway towards a practical, scalable quantum network. For example, ion-photon entanglement with the polarization degree of freedom [4, 24] is most amenable to an optical cavity. An optical cavity can be locked to the $|S_{1/2}, F=1\rangle \leftrightarrow |P_{1/2}, F=1\rangle$ transition of $^{171}\text{Yb}^+$ with the quantization axis along the cavity mode. A weak π -polarized probe on an ion initialized to the $|S_{1/2}, F=0, m_F=0\rangle$ state can excite the

atom to the $|P_{1/2}, F=1, m_F=0\rangle$ level, which is coupled to the $|S_{1/2}, F=1, m=\pm 1\rangle$ ground states through the two polarization modes of the cavity. Such a procedure can produce ion-photon entangled pairs that are useful for ion-photon quantum networks, loophole-free tests of Bell inequalities, and the generation of cluster states.

ACKNOWLEDGMENTS

The authors would like to thank Luis A. Orozco and Howard Carmichael for providing useful insight into cavity QED theory as well as discussions of experimental techniques and system modeling. This work is supported by the US Army Research Office (ARO) with funds from the IARPA MQCO Program and the MURI program on Quantum Optical Circuits of Hybrid Quantum Memories, NSF Physics at the Information Frontier Program, and the NSF Physics Frontier Center at JQI.

-
- [1] R. Blatt and D. J. Wineland, *Nature* **453**, 1008 (2008).
 - [2] L.-M. Duan and C. Monroe, *Rev. Mod. Phys.* **82**, 1209 (2010).
 - [3] D. L. Moehring, P. Maunz, S. Olmschenk, K. C. Younge, D. N. Matsukevich, L.-M. Duan, and C. Monroe, *Nature* **449**, 68 (2007).
 - [4] D. N. Matsukevich, P. Maunz, D. L. Moehring, S. Olmschenk, and C. Monroe, *Phys. Rev. Lett.* **100**, 150404 (2008).
 - [5] S. Olmschenk, D. N. Matsukevich, P. Maunz, D. Hayes, L.-M. Duan, and C. Monroe, *Science* **323**, 486 (2009).
 - [6] P. Maunz, S. Olmschenk, D. Hayes, D. N. Matsukevich, L.-M. Duan, and C. Monroe, *Phys. Rev. Lett.* **102**, 250502 (2009).
 - [7] S. Pironio, A. Acín, S. Massar, A. B. de la Giroday, D. N. Matsukevich, P. Maunz, S. Olmschenk, D. Hayes, L. Luo, T. A. Manning, and C. Monroe, *Nature* **464**, 1021 (2010).
 - [8] A. P. VanDevender, Y. Colombe, J. Amini, D. Leibfried, and D. J. Wineland, *Phys. Rev. Lett.* **105**, 023001 (2010).
 - [9] G. Shu, M. R. Dietrich, N. Kurz, and B. B. Blinov, *Journal of Physics B: Atomic, Molecular and Optical Physics* **42**, 154005 (2009).
 - [10] G. Shu, N. Kurz, M. R. Dietrich, and B. B. Blinov, *Phys. Rev. A* **81**, 042321 (2010).
 - [11] E. W. Streed, B. G. Norton, J. J. Chapman, and D. Kielpinski, *Quantum Information & Computation* **9**, 203 (2009).
 - [12] E. W. Streed, B. G. Norton, A. Jechow, T. J. Weinhold, and D. Kielpinski, *Phys. Rev. Lett.* **106**, 010502 (2011).
 - [13] R. Noek, C. Knoernschild, J. Migacz, T. Kim, P. Maunz, T. Merrill, H. Hayden, C. S. Pai, and J. Kim, *Opt. Lett.* **35**, 2460 (2010).
 - [14] G. Brady, A. Ellis, D. Moehring, D. Stick, C. Highstrete, K. Fortier, M. Blain, R. Haltli, A. Cruz-Cabrera, R. Briggs, J. Wendt, T. Carter, S. Samora, and S. Kemme, *Applied Physics B: Lasers and Optics*, 1 (2011).
 - [15] C. Law and H. Kimble, *Journal of Modern Optics* **44**, 2067 (1997).
 - [16] J. McKeever, A. Boca, A. D. Boozer, R. Miller, J. R. Buck, A. Kuzmich, and H. J. Kimble, *Science* **303**, 1992 (2004).
 - [17] J. I. Cirac, P. Zoller, H. J. Kimble, and H. Mabuchi, *Phys. Rev. Lett.* **78**, 3221 (1997).
 - [18] T. Wilk, S. C. Webster, A. Kuhn, and G. Rempe, *Science* **317**, 488 (2007).
 - [19] B. Weber, H. P. Specht, T. Müller, J. Bochmann, M. Mücke, D. L. Moehring, and G. Rempe, *Phys. Rev. Lett.* **102**, 030501 (2009).
 - [20] G. Guthohrlein, M. Keller, K. Hayasaka, W. Lange, and H. Walther, *Nature* **414**, 49 (2001).
 - [21] A. B. Mundt, A. Kreuter, C. Becher, D. Leibfried, J. Eschner, F. Schmidt-Kaler, and R. Blatt, *Phys. Rev. Lett.* **89**, 103001 (2002).
 - [22] M. Keller, B. Lange, K. Hayasaka, W. Lange, and H. Walther, *Nature* **431**, 1075 (2004).
 - [23] H. G. Barros, A. Stute, T. E. Northup, C. Russo, P. O. Schmidt, and R. Blatt, *New Journal of Physics* **11**, 103804 (2009).
 - [24] L. Luo, D. Hayes, T. A. Manning, D. N. Matsukevich, P. Maunz, S. Olmschenk, J. D. Sterk, and C. Monroe, *Fortschritte der Physik* **57**, 1133 (2009).
 - [25] M. Harlander, M. Brownnutt, W. Hänsel, and R. Blatt, *New Journal of Physics* **12**, 093035 (2010).
 - [26] C. J. Hood, H. J. Kimble, and J. Ye, *Phys. Rev. A* **64**, 033804 (2001).
 - [27] Y. Colombe, “private communication,” (2011).
 - [28] A. Bylinskii and V. Vuletic, “private communication,” (2011).
 - [29] J. J. Childs, K. An, R. R. Dasari, and M. S. Feld, “Single atom emission in an optical resonator,” in *Cavity Quan-*

- tum Electrodynamics*, edited by P. R. Berman (Academic Press, Boston, 1994) pp. 325–380.
- [30] H. J. Kimble, “Structure and dynamics in cavity quantum electrodynamics,” in *Cavity Quantum Electrodynamics*, edited by P. R. Berman (Academic Press, Boston, 1994) pp. 203–266.
 - [31] L. Deslauriers, S. Olmschenk, D. Stick, W. K. Hensinger, J. Sterk, and C. Monroe, Phys. Rev. Lett. **97**, 103007 (2006).
 - [32] S. Olmschenk, K. C. Younge, D. L. Moehring, D. N. Matsukevich, P. Maunz, and C. Monroe, Phys. Rev. A **76**, 052314 (2007).
 - [33] A. E. Siegman, *Lasers* (Stanford University Press, Stanford, 1986).
 - [34] M. L. Terraciano, R. O. Knell, D. L. Freimund, L. A. Orozco, J. P. Clemens, and P. R. Rice, Opt. Lett. **32**, 982 (2007).
 - [35] B. R. Mollow, Phys. Rev. **188**, 1969 (1969).
 - [36] D. Boozer, *Raman Transitions in Cavity QED*, Ph.D. thesis, California Institute of Technology (2005).
 - [37] S. M. Tan, Journal of Optics B: Quantum and Semiclassical Optics **1**, 424 (1999).
 - [38] Y. Zhu, A. Lezama, T. W. Mossberg, and M. Lewenstein, Phys. Rev. Lett. **61**, 1946 (1988).
 - [39] M. Lewenstein and T. W. Mossberg, Phys. Rev. A **37**, 2048 (1988).
 - [40] C. M. Savage, Phys. Rev. Lett. **60**, 1828 (1988).
 - [41] S. Hughes and H. J. Carmichael, Phys. Rev. Lett. **107**, 193601 (2011).
 - [42] M. Baur, S. Filipp, R. Bianchetti, J. M. Fink, M. Göppl, L. Steffen, P. J. Leek, A. Blais, and A. Wallraff, Phys. Rev. Lett. **102**, 243602 (2009).